



Microextraction of lanthanum using a rotating microchannel extractor

SANXING LI, GAOXIANG CHEN, CHUNXIN FAN and JIANHONG LUO*

Department of Chemical Engineering, Sichuan University, Chengdu, Sichuan 610065, China

(Received 23 August, revised 29 September, accepted 6 October 2021)

Abstract: This work introduced a novel microchannel extractor. The extraction system was intended to extract lanthanum nitrate aqueous solution with 2-ethylhexyl phosphoric acid-2-ethylhexyl ester (EHEHPA). Different feeding methods and inner rotors were explored first. The results showed that parallel feeding and inner rotors engraved with spiral stripes were more favorable for extraction. Next, the effect of various factors on the extraction was explored, including the aqueous phase pH, rotational inner rotor speed (R) and the fluid volumetric flow rate (Q). The results showed that these factors are closely related to the extraction. Finally, the experiment was verified by CFD numerical simulation, the simulation result was consistent with the experiment. In this device, active mixing was introduced into the microchannel extraction, which significantly improved the extraction efficiency. Under certain conditions, the extraction efficiency of this device exceeded stirring extraction equilibrium. Moreover, the extraction in the device is faster than with conventional stirring extraction. These advantages provide a possibility for highly efficient extraction of rare earth elements.

Keywords: micro-extraction; La (III); mass transfer; simulation.

INTRODUCTION

Rare earth elements (REEs) are an important non-renewable resource and play an irreplaceable role in high-tech materials. They are widely used in chemical engineering, metallurgy, electronic equipment and other fields.^{1,2} The demand for REEs is also increasing, so the research on extracting and separating them is important. Lanthanides are widely used in many fields because of their luminescence, electronics, and magnetism.³ As one of the most abundant REEs, lanthanum and its compounds are widely used in batteries, catalysts, and so on.⁴

Solvent extraction has the advantages such as: simple equipment, high selectivity, and is renewable.^{5,6} It is widely used in chemical, metallurgy, and other

* Corresponding author. E-mail: luojianhong@scu.edu.cn
<https://doi.org/10.2298/JSC210823080L>

fields.⁷ The separation techniques based on solvent extraction have been widely used to produce high-purity single rare earth solutions or compounds.⁸ However, the conventional equipment like stirring contactors,⁹ packed extraction columns,¹⁰ packed bed columns,¹¹ mixing settlers,¹² etc. can no longer meet the production requirements because of their large area, and a time consuming process. Therefore, it is necessary to develop new equipment. Microchannel extraction is a new direction to improve extraction. Compared with traditional extractors, the specific surface area for a droplet in microchannel is significantly larger. Microchannel extraction has the advantages of large total mass transfer coefficient, short reaction time, safety, etc.¹³ So, it has been a topic of interest for almost 20 years.¹⁴ There have been many reports on micro-extractor, such as tubular microchannel extractor with T-junction,¹⁵ Y-junction serpentine micro-extractor,¹³ hollow fiber contactor¹⁶ and so on. However, two phases are no longer mixed after entering those microreactors. It can be defined as passive mixing. As there are few studies on active mixing micro-extractors, inspired by Nakase *et al.*,^{17,18} our research lab has designed a rotating microchannel extractor.

EXPERIMENTAL

Materials

Kerosene and EHEHPA are purchased from Luoyang Zhongda Chemical Co., Ltd. They are used as diluent and extractant, respectively. After pre-experimental tests, the volume ratio of kerosene to EHEHPA is chosen as 95:5. Lanthanum nitrate (AR) is purchased from Tianjin Oboke Chemical Co., Ltd. Ascorbic acid (AR) and Sudan III (AR) is purchased from Chengdu Jinshan Chemical Reagent Co., Ltd. Hydrochloric acid (AR) is purchased from Sichuan Xilong Science Co., Ltd. Arsenazo (III) is purchased from East China Normal University Chemical Plant (Shanghai). Deionized water is produced by Aquapro water making machine (ABZ1-1001-P) in laboratory. The concentration of lanthanum reserve solution is 510.52 mg L⁻¹.

Experimental equipment and procedure

The schematic diagram of the experimental equipment is shown in Fig. 1.

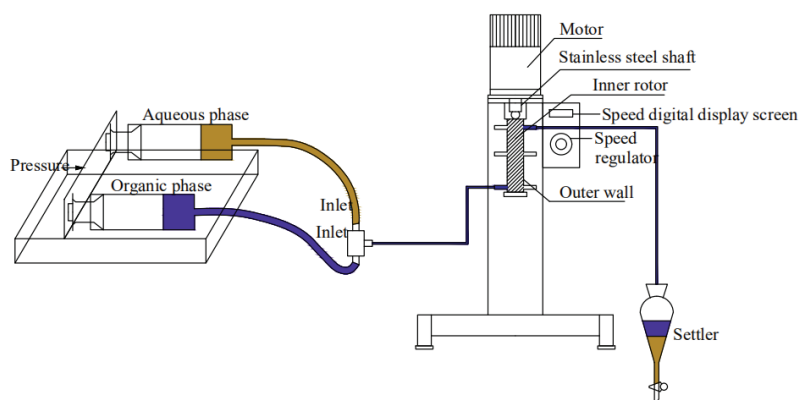


Fig. 1. Schematic drawing of the experimental equipment.

The detailed structure of the extractor is shown in Fig. 2.

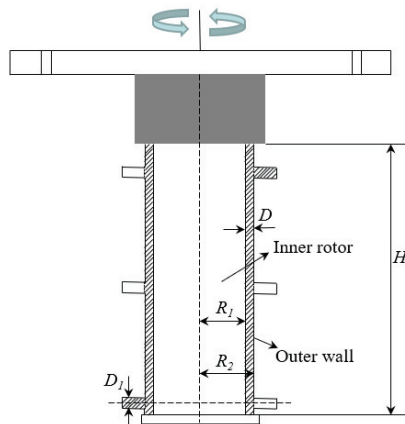


Fig. 2. The detailed structure of extractor.

Radius of inner rotor (R_1) is 9.45 mm; radius of outer cylinder (R_2) is 9.8 mm; making the microchannel width (D) 0.35 mm. The height of fluid region (H) is 200 mm; diameter of inlet/outlet (D_1) is 2.5 mm. The gap between the inner rotor and outer cylinder comprises the microchannel, which is within the standard of microchannel equipment.^{14,19} The inner rotor is connected to a motor for rotation. When the two phases enter the microchannel, they are mixed by the rotation of the inner rotor. This form of active mixing is efficient for mass transfer.²⁰ The outer cylinder is made of hydrophilic acrylic, while the inner rotor is made of hydrophobic polytetrafluoroethylene (PTFE). The design causes the aqueous phase to flow towards the outer wall and the organic phase to flow towards the inner rotor, thereby avoiding emulsification. The inner rotor is replaceable.

There are seven different inner rotors, including a smooth inner rotor (Fig. 3; #0), three inner rotors engraved with cross stripes (Fig. 3; #1, #2 and #3), and three inner rotors engraved with spiral stripes (Fig. 3; #4, #5 and #6).

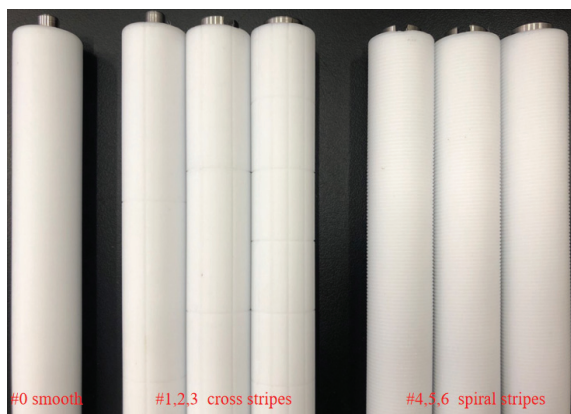


Fig. 3. Different kinds of inner rotors.

All engraved shapes are equilateral triangles, with a height of 0.25 mm, and equidistant. The cross stripes are three horizontal stripes and three vertical stripes (#1), four horizontal

stripes and six vertical stripes (#2), and nine horizontal stripes and twelve vertical stripes (#3). The pitch on the inner rotors with spiral stripes are 1 mm. The difference between them is the helix angle; their details are shown in Fig. 4.

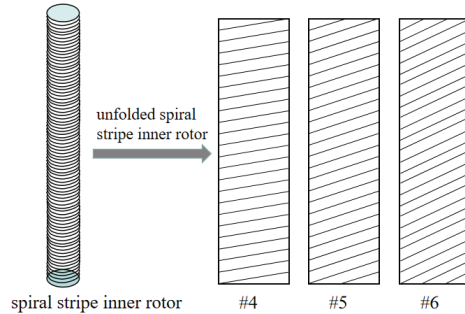


Fig. 4. Schematic diagram of the unfolded spiral stripe inner rotors.

First, different feeding methods and inner rotors were explored. On this basis, the effect of the remaining three factors on extraction was researched. The experiment was run at atmospheric pressure and room temperature. The volume ratio of the two phases (O/A) is 1:1.

Physical properties and analysis

The viscosity of organic phase ($\mu_o = 2.36 \times 10^{-3}$ Pa·s) and aqueous phase ($\mu_{aq} = 9.07 \times 10^{-4}$ Pa·s) are measured with an Ubbelohde viscometer. The surface tension between aqueous phase and organic phase is 22.47 mN m⁻¹, which is measured with an automatic surface tension-meter (BZY-201, Shanghai Fangrui Instrument Co., Ltd.). The two-phase immiscible fluid flow in the microchannel are observed by a high-speed CCD camera (FASTCAM Mini Wx100, Japan Photron). The concentration of La (III) is measured with an ultraviolet spectrophotometer (UV-3100PC, Shanghai Science and Technology Co., Ltd.).

RESULTS AND DISCUSSION

The equations given below are used to analyze the experimental results:

Eq. (1) is used to calculate the percentage extraction:

$$E = 100 \frac{c_{aq,in} - c_{aq,out}}{c_{aq,in}} \quad (1)$$

The overall volumetric mass transfer coefficient ($K_L \alpha$) reflects the mass transfer performance of an extractor. As the component is transferred through the phase interface from one phase to the other, the logarithmic-mean concentration difference (LMCD) was employed to determine the overall volumetric mass transfer coefficient:²¹

$$\Delta_{LMCD} = \frac{(c_{aq,in}^* - c_{aq,in}) - (c_{aq,out}^* - c_{aq,out})}{\ln \left[(c_{aq,in}^* - c_{aq,in}) / (c_{aq,out}^* - c_{aq,out}) \right]} \quad (2)$$

Using LMCD, the average value of the mass transfer flux can be calculated as follows:

$$N = K_L \Delta_{LMCD} \quad (3)$$

$$N = \frac{Q_{\text{aq}}(c_{\text{aq,out}} - c_{\text{aq,in}})}{V\alpha} \quad (4)$$

Incorporating Eqs. (3) and (4), the overall volumetric mass transfer coefficient ($K_L\alpha$) for the extraction process is defined as follows:^{13,21-23}

$$K_L\alpha = \frac{Q}{H\pi(R_2^2 - R_1^2)} \ln \left[\frac{c^{*}_{\text{aq,out}} - c_{\text{aq,in}}}{c^{*}_{\text{aq,out}} - c_{\text{aq,out}}} \right] \quad (5)$$

Eq. (6) is used to calculate the velocity at the inlet and outlet of the fluid:

$$u = \frac{4(Q_{\text{aq}} + Q_o)}{\pi D_l^2} \quad (6)$$

Before evaluating the performance of the device, a conventional stirring extraction experiment was run. When the extraction reached equilibrium, it took 90 s, and $E = 79.61\%$.

Effect of feeding method

The extractor has three inlets and three outlets, as shown in Fig. 2. Different feeding methods were tested using corresponding inlets and outlets, blocking the others with water stop clips. Different feeding methods changed the fluid flow state in the microchannel, affecting the mass transfer. Six different feeding methods were designed, as shown in Fig. 5.

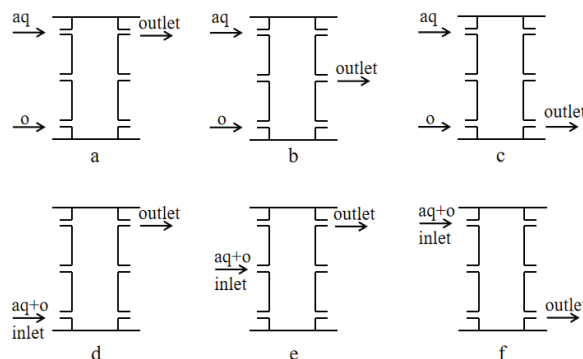


Fig. 5. Different feeding methods. (aq: aqueous phase; o: organic phase).

For a, b and c, the idea was that the density of aqueous phase was greater than organic phase. Feeding from above makes the aqueous phase flow downward. Similarly, the organic phase flows upward to achieve a countercurrent flow. For d, e and f, a parallel feeding method was used. All outlets were designed to ensure that the fluid stays in the microchannel longer.

Methods d, e and f performed significantly better than methods a, b and c, as shown in Fig. 6. The flow patterns of all methods are shown in Fig. 7.

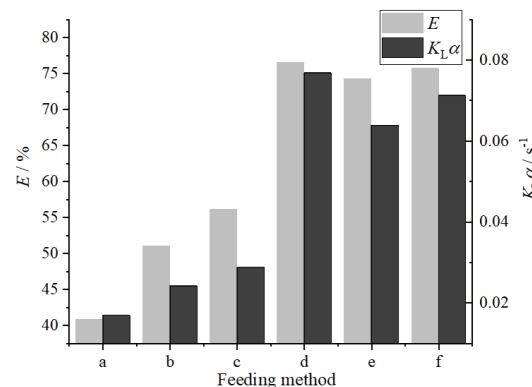


Fig. 6. Variation of E and $K_{L\alpha}$ with feeding method. Conditions: inner rotor is #0, $Q_{\text{aq}} = 3 \text{ mL min}^{-1}$, $R = 400 \text{ rpm}$.

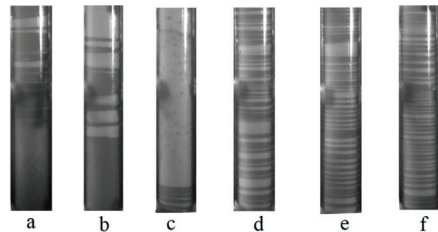


Fig. 7. Flow patterns of different feeding methods. Conditions: inner rotor is #0, $Q_{\text{aq}} = 3 \text{ mL min}^{-1}$, $R = 400 \text{ rpm}$.

The dark part was the organic phase dyed with Sudan III, and the aqueous phase was the transparent part without dyeing. In method a, because fluid is discharged from above, the rising organic phase can only contact the initially deposited aqueous phase, and the subsequent aqueous phase is not fully extracted before being discharged. In method b, fluid is discharged from the middle, causing the upper part to be filled with the aqueous phase and the lower part filled with the organic phase, while the two phases were mixed briefly around the outlet. In method c, fluid was discharged from the bottom, the residence time was short, the organic phase could not flow upward as expected, and it was discharged before being fully extracted. For these reasons, feeding methods a, b and c did not perform well. In methods d, e, and f, parallel flow causes the two phases to be fed together and discharged together so that they mix well and disperse evenly. Moreover, the flow distance of the parallel flow is longer, causing it to perform significantly better. Based on the results, feeding method d was chosen for the next experiment.

Effect of inner rotor surface smoothness

There are seven inner rotors, as shown in Fig 3. The effect of inner rotor surface smoothness on extraction was explored. The results are shown in Fig. 8.

The engraved inner rotors are conducive to extraction. This phenomenon can be explained in three ways. First, because the engravings are equilateral triangles, the engraved inner rotor has a larger wetted area than the smooth one. The increased wetted area is conducive to liquid-liquid contact mass transfer. Second,

the rough engravings allow the fluid to be dispersed and mixed, thereby increasing the surface renewal of the droplet. Third, the engravings increase the turbulence of the fluid. These changes had a positive effect on the extraction. The inner rotors engraved with spiral stripes perform better than those engraved with cross stripes because they have a larger wetted area (mentioned before as the first explanation).

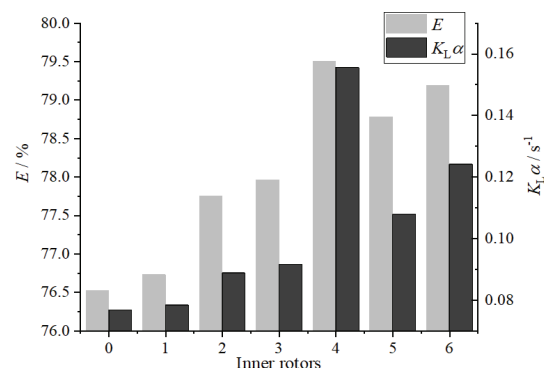
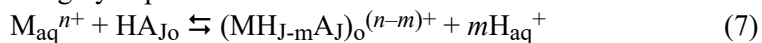


Fig. 8. Variation of E and $K_L\alpha$ with inner rotor surface smoothness. Conditions: feeding method is d, $Q_{aq} = 3$ mL min⁻¹, $R = 400$ rpm.

Effect of aqueous phase pH

EHEHPA is an acidic extractant and contains dissociable H^+ , its mechanism for extracting metal cations is consistent with the cation exchange mechanism. The mechanism is roughly expressed as follows:



The subscripts aq and o represent the aqueous and organic phases, respectively. J represents the number of polymerizations of the extractant, and m is the number of solvent molecules of EHEHPA in the extraction complex.

The apparent equilibrium constant K can be expressed as follows:

$$K = \frac{c_{(MH_{J-m}A_J)_o^{(n-m)+}} c_{H_{aq}}^{+m}}{c_{M_{aq}}^{n+} c_{HA_{Jo}}} \quad (8)$$

The distribution coefficient of metal ions in solution can be expressed as follows:

$$D = \frac{c_{(MH_{J-m}A_J)_o^{(n-m)+}}}{c_{M_{aq}}^{n+}} \quad (9)$$

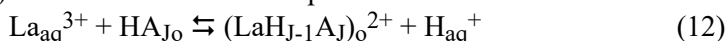
pH definition is as follows:

$$pH = -\log c_{H^+} \quad (10)$$

Combining Eqs. (8)–(10), Eq. (11) can be obtained:

$$\log D = \log (Kc_{(HA)J_0}) + mpH \quad (11)$$

To explore the mechanism the experiment was run in the pH range from 1.5 to 2.5. The linear relationship between $\log D$ and pH is shown in Fig. 9a. The slope of this line is 1.09681 ± 0.09847 , which is close to 1, indicating that the number of solvent molecules of the extracted complex in the organic phase is equal to 1 ($m = 1$).²⁴ Therefore, when pH ranges from 1.5 to 2.5, the mechanism of extracting La (III) with EHEHPA can be expressed as follows:



The effect of pH, in a larger range, on extraction was explored next. The results are shown in Fig. 9b. As the pH of aqueous phase increases from 1.5 to 5.1 (with 5.1 being the initial pH of aqueous phase), E does as well. The change in trend is the same as the mechanism above. As the pH increases, E increases slowly. When the pH is about 3.5, E begins to stabilize.

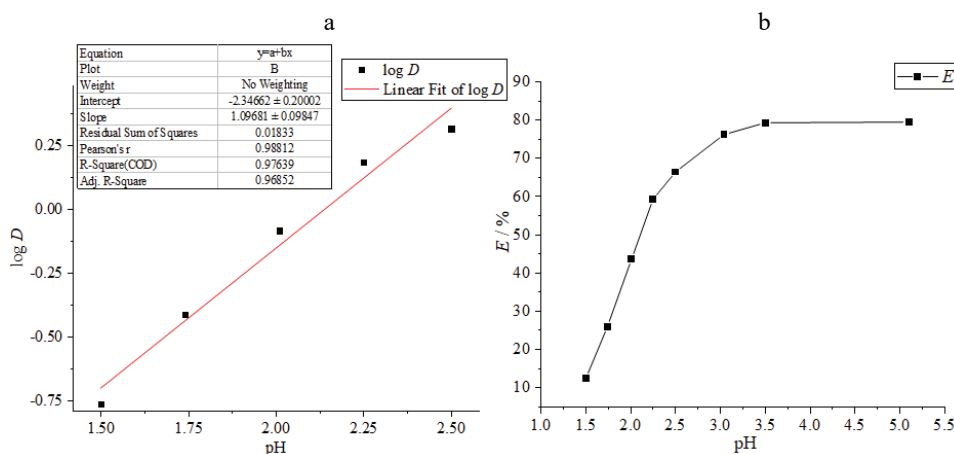


Fig. 9. Research on pH. a) Extraction distribution coefficient ($\log D$) versus the pH; b) variation of E with the pH of aqueous phase. Conditions: feeding method is d, inner rotor is #4, $R = 400$ rpm, $Q_{\text{aq}} = 3 \text{ mL min}^{-1}$.

Effect of inner rotor speed

The experiment was done without rotating at first, and then the speed of the inner rotor was set from 50 to 600 rpm to explore the effect of active mixing on the extraction, Fig. 10.

Without rotation $E = 57.60 \%$ and $K_L \alpha = 3.040 \times 10^{-2} \text{ s}^{-1}$. E reaches 75.93 % and $K_L \alpha$ reaches $7.265 \times 10^{-2} \text{ s}^{-1}$ at a speed of 50 rpm. Compared to the passive mixing without rotation, the active mixing produced by rotating the inner rotor greatly improves extraction. When the inner rotor is at rest, the fluid track is 200 mm long from bottom to top. The schematic diagram of force on the fluid when the inner rotor rotates is shown in Fig. 11.

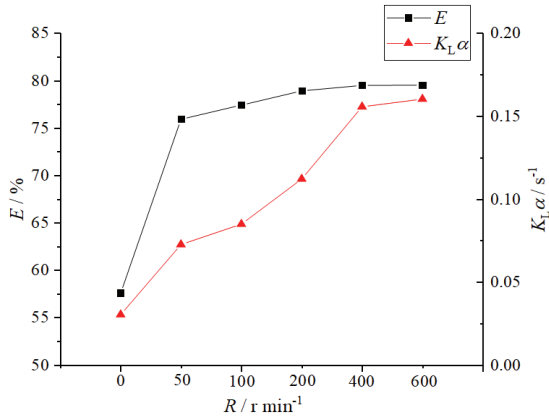


Fig. 10. Variations of E and $K_{L\alpha}$ with inner rotor speed. Conditions: feeding method is d, inner rotor is #4, $Q_{\text{aq}} = 3 \text{ mL min}^{-1}$.

F_1 represents the upward force on the fluid, which mainly comes from the liquid that subsequently enters the microchannel, F_2 represents the centrifugal force, G represents gravity, and F is the total force on the fluid. As F is inclined upward, the fluid spirals up in the microchannel, and its flow pattern is shown in Fig. 12.

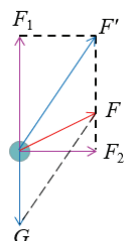


Fig. 11. The schematic diagram of force on the fluid.

The length of this motion track is greater than 200 mm. A longer motion track increases the contact area, and active mixing increases the turbulence of the fluid.

When the inner rotor is at rest, the two phases are not dispersed well and aggregate into large blocks, as shown in Fig. 12.

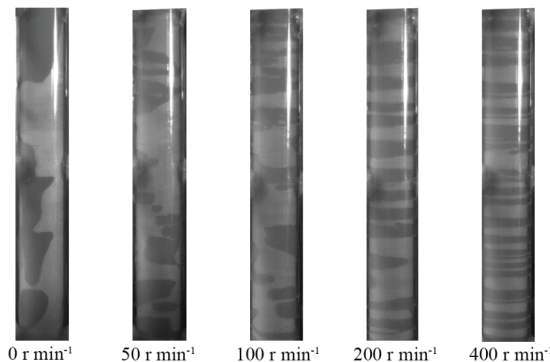


Fig. 12. Flow patterns of different inner rotor speed. Conditions: feeding method is d, inner rotor is #4, $Q_{\text{aq}} = 3 \text{ mL min}^{-1}$.

When the inner rotor rotates, the two phases gradually become increasingly dispersed as the speed increases. Dispersion is conducive to mass transfer, causing the extraction efficiency to increase. As the rotation speed reaches 200 rpm, the dispersion gradually becomes stable, and the extraction efficiency is relatively stable.

This is because centrifugal force determines the size of the droplet in the microchannel. The higher rotation speed causes the smaller droplet size, and the organic droplets are more easily dispersed in the aqueous phase. However, there is a limit to this relationship; as the rotation speed increases and the droplet size decreases to a certain level, it cannot be reduced. Therefore, even if the rotation speed continues to increase, the mass transfer cannot increase significantly, and the extraction efficiency remains stable.

Effect of fluid volumetric flow rate

Changing the fluid volumetric flow rate while keeping other conditions unchanged was tested. Fig. 13 shows the effect of the fluid volumetric flow rate on E . As Q_{aq} increases from 0.5 to 5.0 mL min^{-1} , E decreases.

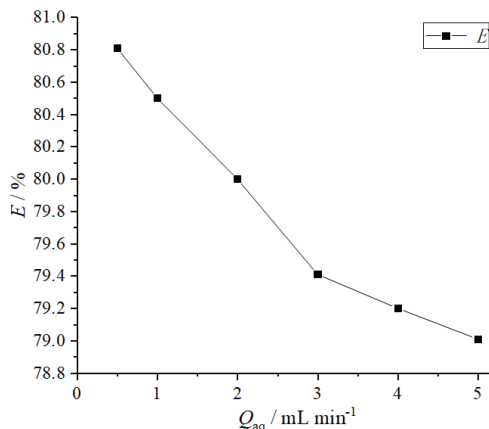


Fig. 13. Variation of E with fluid volumetric flow rate. Conditions: feeding method is d, inner rotor is #4, $R = 400$ rpm.

Fig. 14 shows, as the flow rate increases, the fluid becomes more dispersed, which helps mass transfer. This happens because increasing Q helps to renew the phase interface. However, the extraction efficiency is reduced as the residence time of the fluid decreases. The magnitude of the reduction in residence time outweighs the increase in the mass transfer rate, causing the overall extraction efficiency to be reduced.

It is worth noting that when Q_{aq} is reduced to a certain level, such as 0.5 mL min^{-1} , the extraction efficiency of the extractor exceeds the equilibrium value of stirring extraction. This happens for two reasons. One, when Q is small, the residence time is extended. As they stay for a long time, the different densities of the

two phases are separated. As a result, there are several intermittent fluid accumulation bands during the slow rise of the fluid, as shown in Fig. 14 (0.5 mL). Each time the fluid passes through an accumulation band, an extraction is completed. In other words, it creates a situation like multi-stage extraction. On the other hand, the fluid forms a thin liquid film at a low flow rate, which is conducive to mass transfer.

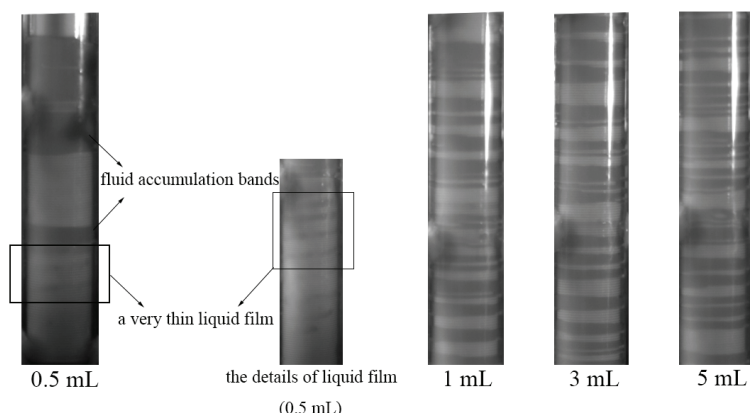


Fig. 14. Flow patterns at different volumetric flow rate conditions: feeding method is d, inner rotor is #4, $R = 400$ rpm.

CFD simulation of flow pattern

After the experiment, CFD numerical simulation was carried out. The software used was SolidWorks 2020 to build the model, IECM CFD 19.2 to draw the mesh and ANSYS Fluent 19.2 to simulate the fluid flow. The mesh is unstructured, and the number is about 3.52 million.

All simulations use double-precision transient solver. The volume of fluid method (VOF) is used to model the two-phase interface. The transient simulation uses the explicit VOF method, and the time step of the volume fraction equation is limited by the maximum Courant number.⁷ The multi-reference Frame (MRF) model is used to model the device, that is the microchannel divided into two areas, one is the area a near the inner rotor, the other is the area b near the acrylic outer cylinder. The fluid in the area a is mainly moved by the rotation of the inner rotor, and the fluid in the area b moves with the fluid in the area a. In the simulation, the time step is controlled at 10^{-5} – 3×10^{-5} s. Momentum is discretized by a second order upwind method. During the calculation process, the Courant number is kept below 5 by adjusting momentum to ensure the convergence of result.

The simulation result is shown in Fig. 15, and the result is basically consistent with the fluid flow pattern captured by the high-speed camera.

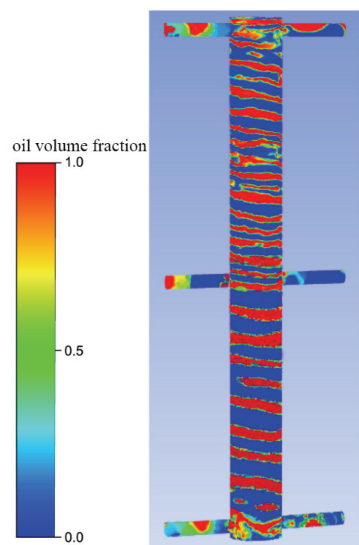


Fig. 15. Simulation result of fluid flow pattern in outer cylinder side Conditions: feeding method is d, inner rotor is #4, $Q_{\text{aq}} = 3 \text{ mL min}^{-1}$, $R = 400 \text{ rpm}$.

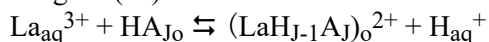
CONCLUSION

In this work, a novel rotating microchannel extractor was used to extract La (III). The introduction of active mixing generated by the rotation of the inner rotor caused the microchannel extraction device to perform excellently. First, the feeding methods and the inner rotors were researched. Next, the effects of aqueous phase pH, inner rotor speed and fluid volumetric flow rate on extraction were investigated. Finally, the experiment was verified by CFD numerical simulation. The experimental results obtained are as follows:

1. Active mixing increases the fluid's turbulence and the surface renewal rate of the mixed-phase. Active mixing significantly improves the extraction in the microchannel.

2. For this novel extractor, the best feeding method is d, a parallel feeding method involving feeding in the bottom and discharging from the top. The best inner rotor is spiral tube #4. The increase in inner rotor speed and the aqueous phase pH is beneficial to extraction. Conversely, an increase in fluid volumetric flow rate is not conducive to extraction.

3. When the pH of the aqueous phase ranges from 1.5 to 2.5, the reaction mechanism for extracting La (III) with EHEHPA can be described as:



4. The extraction in this device is faster than the conventional stirring extraction. When the residence time of the device is 25.38 s, $E = 79.01 \%$, which has basically reached the extraction equilibrium, while stirring extraction takes 90 s.

5. The numerical simulation results are consistent with the phenomena observed in the experiment, which further supports the experiment.

6. When the fluid volumetric flow rate is low, the extraction efficiency of the extractor exceeds the equilibrium value of stirring extraction. It provides a possibility for highly efficient extraction of rare earth elements.

Acknowledgements. We gratefully acknowledge financial support from the National Natural Science Foundation of China (21776181), Sichuan University innovation spark project (2018SCUH0012), Science and Technology Plan Project of Sichuan Province (2021YFG0285) and Chinese National Key Research and Development Plan (2018YFC1900203-03).

ИЗВОД

МИКРОЕКСТРАКЦИЈА ЛАНТАНА ПОМОЋУ РОТИРАЈУЋЕГ МИКРОКАНАЛНОГ ЕКСТРАКТОРА

SANXING LI, GAOXIANG CHEN, CHUNXIN FAN и JIANHONG LUO

Department of Chemical Engineering, Sichuan University, Chengdu, Sichuan 610065, China

У овом раду описан је нови микроканални екстрактор. Екстракциони систем је коришћен за екстракцију воденог раствора лантан-нитрата коришћењем 2-етилхексил-естра 2-етилхексил-фосфорне киселине (ЕНЕНРА). У експериментима су испитивани различити начини увођења напојних смеша, као и различити типови унутрашњих ротора. Испитивања су показала да се најбољи резултати постижу приликом паралелног увођења напојних смеша и коришћењем унутрашњих ротора са спиралним жљебовима. Такође је испитиван утицај процесних параметара, као што су pH вредност раствора, број обртаја унутрашњег ротора (R) и запремински проток флуида (Q) на ефикасност процеса. Резултати су показали да сви ови фактори значајно утичу на процес екстракције. Експериментални резултати су верификовани CFD нумеричком симулацијом. У овом уређају се врши активно мешање струја у микроканалном екстрактору, што значајно доприноси повећању ефикасности процеса. Под одређеним условима извођења, ефикасност екстракције је већа од равнотежне екстракције у класичном уређају са мешалицом. Такође, екстракција у овом уређају се одвија већом брзином у односу на класичан уређај. Ове предности омогућавају коришћење микроканалног екстрактора за извођење високо-ефикасне екстракције елемената из групе ретких земаља.

(Примљено 23. августа, ревидирано 29. септембра, прихваћено 6. октобра 2021)

REFERENCES

1. R. K. Jyothi, T. Thenepalli, J. W. Ahn, P. K. Parhi, K. W. Chung, J. Y. Lee, *J. Clean Prod.* **267** (2020) 122048 (<http://dx.doi.org/10.1016/j.jclepro.2020.122048>)
2. A. Soukeur, A. Szymczyk, Y. Berbar, M. Amara, *Sep. Purif. Technol.* **256** (2021) 117857 (<http://dx.doi.org/10.1016/j.seppur.2020.117857>)
3. V. V. Belova, M. M. Martynova, Y. V. Tsareva, V. E. Baulin, D. V. Baulin, *J. Mol. Liq.* **293** (2019) 111568 (<http://dx.doi.org/10.1016/j.molliq.2019.111568>)
4. R. Panda, M. K. Jha, J. Hait, G. Kumar, R. J. Singh, K. Yoo, *Hydrometallurgy* **165** (2016) 106 (<http://dx.doi.org/10.1016/j.hydromet.2015.10.019>)
5. W. Xiang, S. Liang, Z. Zhou, W. Qin, W. Fei, *Hydrometallurgy* **171** (2017) 27 (<http://dx.doi.org/10.1016/j.hydromet.2017.04.007>)

6. C. Shi, D. Duan, Y. Jia, Y. Jing, *J. Mol. Liq.* **200** (2014) 191 (<http://dx.doi.org/10.1016/j.molliq.2014.10.004>)
7. R. Ma, C. Fan, Y. Wang, J. Luo, J. Li, Y. Ji, *Chem. Eng. Process.* **151** (2020) 107916 (<http://dx.doi.org/10.1016/j.cep.2020.107916>)
8. F. Xie, T. A. Zhang, D. Dreisinger, F. Doyle, *Miner. Eng.* **56** (2014) 10 (<http://dx.doi.org/10.1016/j.mineng.2013.10.021>)
9. P. A. Quadros, C. M. S. G. Baptista, *Chem. Eng. Sci.* **58** (2003) 3935 ([http://dx.doi.org/10.1016/S0009-2509\(03\)00302-6](http://dx.doi.org/10.1016/S0009-2509(03)00302-6))
10. A. M. Dehkordi, *Ind. Eng. Chem. Res.* **40** (2001) 681 (<http://dx.doi.org/10.1021/ie000279s>)
11. R. P. Verma, M. M. Sharma, *Chem. Eng. Sci.* **30** (1975) 279 ([http://dx.doi.org/10.1016/0009-2509\(75\)80078-9](http://dx.doi.org/10.1016/0009-2509(75)80078-9))
12. M. N. Kashid, I. Gerlach, S. Goetz, J. Franzke, J. F. Acker, F. Platte, D. W. Agar, S. Turek, *Ind. Eng. Chem. Res.* **44** (2005) 5003 (<http://dx.doi.org/10.1021/ie0490536>)
13. Y. He, K. Chen, C. Srinivasakannan, S. Li, S. Yin, J. Peng, *Chem. Eng. J.* **354** (2018) 1068 (<http://dx.doi.org/10.1016/j.cej.2018.07.193>)
14. K. Wang, G. Luo, *Chem. Eng. Sci.* **169** (2017) 18 (<http://dx.doi.org/10.1016/j.ces.2016.10.025>)
15. G. Orsi, M. Roudgar, E. Brunazzi, C. Galletti, R. Mauri, *Chem. Eng. Sci.* **95** (2013) 174 (<http://dx.doi.org/10.1016/j.ces.2013.03.015>)
16. D. N. Ambare, S. A. Ansari, M. Anitha, P. Kandwal, D. K. Singh, H. Singh, P. K. Mohapatra, *J. Membr. Sci.* **446** (2013) 106 (<http://dx.doi.org/10.1016/j.memsci.2013.06.034>)
17. M. Nakase, R. Makabe, K. Takeshita, *J. Nucl. Sci. Technol.* **50** (2013) 287 (<http://dx.doi.org/10.1080/00223131.2013.772445>)
18. M. Nakase, H. Kinuhata, K. Takeshita, *J. Nucl. Sci. Technol.* **50** (2013) 1089 (<http://dx.doi.org/10.1080/00223131.2013.835248>)
19. C. Xu, T. Xie, *Ind. Eng. Chem. Res.* **56** (2017) 7593 (<http://dx.doi.org/10.1021/acs.iecr.7b01712>)
20. P. Erfle, J. Riewe, H. Bunjes, A. Dietzel, *Micromachines* **10** (2019) 220 (<http://dx.doi.org/10.3390/mi10040220>)
21. Q. Li, P. Angeli, *Chem. Eng. Sci.* **143** (2016) 276 (<http://dx.doi.org/10.1016/j.ces.2016.01.004>)
22. S. Yin, J. Pei, J. Peng, L. Zhang, C. Srinivasakannan, *Hydrometallurgy* **175** (2018) 64 (<http://dx.doi.org/10.1016/j.hydromet.2017.10.027>)
23. J. Chang, F. Jia, C. Srinivasakannan, K. A. Mumford, X. Yang, *Chem. Eng. Process.* **137** (2019) 54 (<http://dx.doi.org/10.1016/j.cep.2019.02.001>)
24. S. Dai, J. Luo, J. Li, X. Zhu, Y. Cao, S. Komarneni, *Ind. Eng. Chem. Res.* **56** (2017) 12717 (<http://dx.doi.org/10.1021/acs.iecr.7b01888>).